RSC Advances

PAPER

View Article Online
View Journal | View Issue



Cite this: *RSC Adv.*, 2018, **8**, 3919

# Sanguinarine and chelerythrine: two natural products for mitochondria-imaging with aggregation-induced emission enhancement and pH-sensitive characteristics†

Yaohui Lei,[a] Liyan Liu,[a] Xuemei Tang,[a] Depo Yang,[a] Xuhui Yang*[b] and Feng He *[a]

In this paper, two natural products: chelerythrine (Che) and sanguinarine (San) were systematically explored for aggregation-induced emission enhancement (AIEE) characteristics by a series of spectroscopic and theoretical experiments. After adding increasing amounts of $H_2O$ into $CH_3OH$ solutions of San and Che, typical AIEE behaviors could be observed; then, the enhanced fluorescence lifetime and nanoparticles were also monitored. Moreover, owing to the presence of two kinds of molecular conformations, the pH-sensitive behaviors of San and Che were displayed in $CH_3OH/H_2O$ mixtures. Density functional theory indicated that J-aggregation was responsible for the AIEE behaviors of San and Che. Taking advantage of the unique AIEE characteristics, excellent cellular permeability and mitochondria-targeting ability of Che were displayed as a lipophilic cation. In addition, based on the remarkable anti-cancer activity *in vitro*, depolarization of the mitochondrial membrane potential and the morphological collapses of mitochondria caused by Che were observed, confirming that the aggregation of Che in mitochondria could result in mitochondrial dysfunction. Herein, San and Che are proposed to be AIEE dyes for promising mitochondria-imaging which enabled us to observe their anti-cancer effects directly. In conclusion, these natural products provided an innovative strategy for potential image-guided therapy of tumor cells.

Received 30th November 2017
Accepted 8th January 2018

DOI: 10.1039/c7ra12920c

rsc.li/rsc-advances



## Introduction

As the principal energy-producing organelles in eukaryotic cells, mitochondria are vital sub-cellular compartments where cellular respiration takes place.[1] By a series of electron-transport systems in the oxidative phosphorylation pathway,[2] mitochondria can regulate enormous metabolic functions, such as producing most of the cellular ATP, regulating the cellular redox state, generating most of the cellular reactive oxygen species (ROS), and initiating cellular apoptosis.[3] Therefore, mitochondria-targeting molecules have attracted a lot of research interests for manipulating mitochondrial functions,[4] which associate with many human diseases including cancer, cardiopathy, Alzheimer's disease, and diabetes.[5–9] Studies have shown that mitochondria can keep a constant membrane potential of about −180 mV across lipid bilayers by ion channels.[10,11] This remarkably negative potential can distinguish mitochondria from other intracellular counterparts and facilitate lipophilic cations diffusing into mitochondria selectively by an electrostatic driving force. Nowadays, numerous lipophilic cations have been successfully explored for mitochondrial targeting; for instance, triphenylphosphonium (TPP), pyridine group, quinoline moiety, and peptides with arginine.[12] In particular, TPP is a typical mitochondria-targeting group which has been conjugated with many fluorogens and drugs, enabling delivery of various molecules into mitochondria.[13] However, such modifications have risks of altering the pathway of reagents and even changing their properties, so it's still highly desirable to explore new reagents which possess mitochondria-targeting characteristics.

Optical dyes, especially fluorescent dyes, have been powerful tools for mitochondria-imaging.[14] Conventional mitochondrial fluorescent dyes, such as rhodamine, lanthanide complexes, boron-dipyrromethene, and mitotracker dyes, have been successfully developed to label mitochondria selectively. They display high specificity, high spatial resolution, and excellent sensitivity to mitochondria. Unfortunately, due to the notorious aggregation-caused quenching (ACQ) effect, these dyes are only used in low concentrations and thus can be easily photobleached in a mitochondrial imaging process. To solve this problem, a series of fluorogens undergoing aggregation-induced emission enhancement (AIEE) characteristics have

[a]*Department of Medicinal Chemistry, School of Pharmaceutical Science, Sun Yat-sen University, Guangzhou, 510006, P. R. China. E-mail: hefeng@mail.sysu.edu.cn*

[b]*Assisted Reproductive Center, Guangdong Women and Children's Hospital, Guangzhou, 510010, P. R. China. E-mail: yxhshy52@163.com*

† Electronic supplementary information (ESI) available. See DOI: 10.1039/c7ra12920c

been explored since the AIE(E) phenomenon was first reported by Tang in 2001.[15] Contrary to traditional ACQ, AIE(E)-active dyes are weakly emissive in a dilute solution, but can emit intense emissions in the aggregated state.[16,17] Because of their satisfactory anti-photobleaching abilities and excellent labelling properties, various AIE(E)-active dyes have been developed for bioanalysis and bioimaging applications.[18] In particular, Tang's group reported the first AIE-active probe for mitochondrial imaging and tracking by embedding the TPP group into the tetraphenylethene (TPE) fluorophore.[19] Furthermore, they also reported several AIE-active mitochondria probes and targeting drug delivery systems.[20–23] Recently, AIE(E)-active reagents for simultaneous targeting, imaging, and treatment have grown dramatically because of their multifunctional properties.[24] They can not only produce a fluorescence signal in some specific organelles, but also improve therapeutic efficiency. Liu's group reported the first AIE-active reagent (AIE-mito-TPP) for mitochondrial targeting, imaging, and treatment in cancer therapy.[25] This multifunctional reagent provides an innovative strategy for potential image-guided therapy of tumor cells. Inspired by that finding, several AIE(E)-active reagents containing a mitochondria-targeting group and an anti-cancer agent have been successfully fabricated.[26–28] However, despite the fact that several similar reagents have been reported, studies on exploring new AIE(E)-active fluorogens for mitochondria-targeting therapy of tumor cells are still limited. Therefore, the development of AIE(E)-active reagents with mitochondria-targeting ability and anti-cancer effect is highly desirable to track them and visualize their therapeutic effects directly.

As two well characterized benzophenanthridine alkaloids, chelerythrine (Che) and sanguinarine (San) display a broad spectrum of pharmacological activities, including anti-inflammatory, anti-bacterial, and anti-cancer activities.[29] Numerous pharmacological reports have described their inhibitory effects on mitochondrial energy coupling as activators of reactive oxygen species (ROS), demonstrating they are effective inducers of apoptosis in a variety of cancer cell lines.[30,31] However, though the actions of Che and San on tumor cells, as well as their underlying mechanisms, have been explored widely, the mitochondrial changes during the process are still confusing. Based on their proven anti-cancer properties and our previous research,[32–35] the AIEE properties and pH-sensitive behaviors of Che and San were discovered in this study. With the advantage of a unique fluorescence characteristic, Che is reported to light up the mitochondrial region specifically for the first time. More importantly, in combination with its remarkable anti-cancer effect, Che was applied successfully to induce mitochondrial dysfunction in a short period of time, including depolarization of the mitochondrial membrane potential and the morphological collapses of mitochondria. In this paper, the AIEE-based organic small molecules provide novel insights into their anti-cancer effects in virtue of mitochondria-targeting imaging and make it possible to develop new image-guided therapeutic reagents.

# Results and discussion

### Aggregation-induced emission enhancement properties

San and Che are soluble in pure $CH_3OH$ solution, while insoluble in $H_2O$. With regard to AIEE properties, absorption and emission spectra of San and Che in $CH_3OH/H_2O$ mixed solvents were studied. As we can see in Fig. 1a, San is well dispersed in pure $CH_3OH$ solvent with a structured absorption spectrum. However, when the ratio of water increases, the absorption curve of San in the poorer solvents is narrowed at 330 nm and an acromion appears at 349 nm. Moreover, a level-off tail can be seen in the visible region with the increasing water ratio (commonly found in nanoparticle suspensions), indicative of the formation of aggregates of San due to the Mie effect.[36] Furthermore, an intense fluorescence enhancement can be observed at 582 nm with the increasing water fraction until reaching its maximum value at 80%. This trend is commonly observed in AIEE-active dyes, confirming the unique AIEE behavior of San. Meanwhile, the emission spectra exhibit a large red shift from 465 nm to 582 nm and the fluorescence color in solution changes from dark blue to yellow under a UV lamp (365 nm). The color change is visible, which also provides evidence for the AIEE property of San. However, when the percentage of water fraction further reaches 90%, the fluorescence emission at 582 nm decreases due to the formation of greater particles which can reduce the effective concentrations of light-emitting nanoparticles. In summary, as displayed in Fig. 1, the AIEE phenomenon of San occurs at 582 nm when the percentage of water fraction is less than 80%. Interestingly, a similar AIEE behavior of Che in $CH_3OH/H_2O$ mixed solvents is also observed in Fig. 2. When the percentage of the poor solvent increases from 0 to 90 vol%, the absorption curve of Che is narrowed at 320 nm and an acromion appears at 338 nm. At the same time, a level-off tail in the visible region can be seen. These facts give us a hint that light-emitting nanoparticles have been formed in the poorer solvent. Importantly, the fluorescence emission intensity of Che at 570 nm increases drastically and reaches its maximum value at 90% with the percentage of water fractions changing from 30 to 90 vol%. Besides, as illustrated in Fig. 2b, the fluorescence color in solution changes from dark blue to yellow under a UV lamp at 365 nm. All the above results suggest Che also exhibits an excellent AIEE property (Scheme 1).

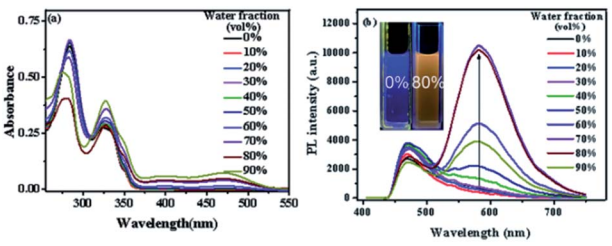


Fig. 1 Absorption and emission spectra of San in $CH_3OH/H_2O$ mixtures with different water fractions (0–90 vol%). (a) Absorption spectra of San ($c = 2.07 \times 10^{-5}$ M) in $CH_3OH/H_2O$ mixtures. (b) Fluorescence emission spectra of San ($\lambda_{ex} = 385$ nm) in $CH_3OH/H_2O$ mixtures. Inset: photographs of San (20 μM) with 0 vol% and 80 vol% water fractions under a UV lamp (365 nm).

 

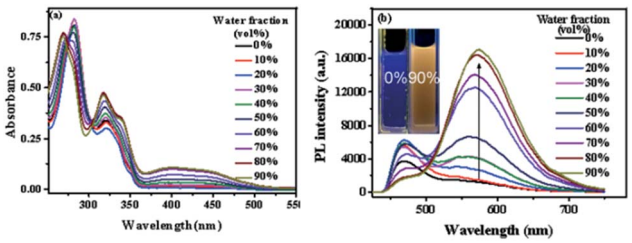


Fig. 2 Absorption and emission spectra of Che in $CH_3OH/H_2O$ mixtures with different water fractions (0–90 vol%). (a) Absorption spectra of Che ($c = 2.07 \times 10^{-5}$ M) in $CH_3OH/H_2O$ mixtures with different water fractions (0–90 vol%). (b) Fluorescence emission spectra of Che ($\lambda_{ex} = 380$ nm) in $CH_3OH/H_2O$ mixtures with different water fractions (0–90 vol%). Inset: photographs of Che (20 μM) with 0 vol% and 90 vol% water fractions under a UV lamp (365 nm).

Studies have shown that San and Che undergo an equilibrium involving two kinds of molecular conformations in solution: a non-ionic form and a quaternary ammonium salt form as shown in Scheme 2, which are in accordance with the two peaks in the spectra. Specifically, the emission maximum at about 450 nm corresponds to the non-ionic form which displays blue fluorescence emission, while the emission peak at about 580 nm corresponds to the quaternary ammonium salt form which emits yellow-green fluorescence.[37] In the emission spectra of San and Che, the fluorescence intensity at 580 nm increases drastically with an increase in water fractions, while the fluorescence intensity at about 450 nm shows negligible changes with the increasing water ratio. The spectra indicate that the AIEE phenomena of San and Che occur at 580 nm which corresponds to the quaternary ammonium salt form. Based on the presence of two kinds of molecular conformations in solution, the spectra indicate that the quaternary ammonium salt forms of San and Che are responsible for AIEE behaviors at 580 nm.

Another superior feature of AIEE-active molecules is an enhancement of fluorescence lifetime in the aggregated state. As displayed in Table 1, the fluorescence lifetime data of San in the $CH_3OH$, $CH_3OH/H_2O$ (5 : 5 v/v) mixture and $CH_3OH/H_2O$ (2 : 8 v/v) mixture are 2.76 ns, 3.05 ns, and 3.40 ns, respectively. The fluorescence lifetime of San increases gradually with an increase in water fractions, which is consistent with the fluorescence emission spectra of San. Che displays a similar phenomenon compared with San; the fluorescence lifetime data in the $CH_3OH$, $CH_3OH/H_2O$ (5 : 5 v/v) mixture, and $CH_3OH/H_2O$ (1 : 9 v/v) are 2.95 ns, 3.17 ns, and 3.27 ns, respectively. The increasing trend is also in accordance with the fluorescence emission spectra of Che as mentioned above. Moreover, the TEM images confirm the formation of nanoparticles of San and Che with different water ratios.

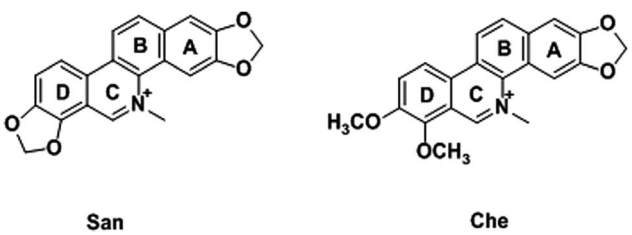


Scheme 1 The structures of sanguinarine and chelerythrine.

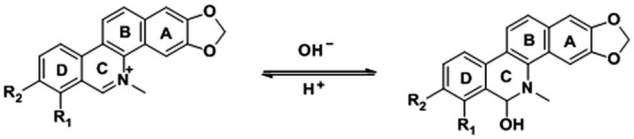


Scheme 2 The equilibrium of the non-ionic form and the quaternary ammonium salt form of San and Che in solution.

As we can see in Fig. 3, many cubic nanoparticles with diameters of 200–400 nm can be clearly visualized. Furthermore, with water fractions increasing, the sizes of these nanoparticles gradually become bigger. These facts give us a direct visualization of the formation of nanoparticles during the process. Moreover, in virtue of the remarkable AIEE properties of San and Che, photostability is measured during 1 h. Fig. S1† shows the time courses of fluorescence intensity of San (20 μM) in a $CH_3OH/H_2O$ (2 : 8 v/v) mixture and Che (20 μM) in a $CH_3OH/H_2O$ (1 : 9 v/v) mixture. The fluorescence intensity was measured at $\lambda_{ex/em} = 385/582$ nm of San and $\lambda_{ex/em} = 380/570$ nm of Che. As shown in Fig. S1,† the results indicate that San and Che possess good photostability.

## PH-sensitive behaviors

As shown in Scheme 2, most of San and Che exist in quaternary ammonium salt forms in acidic solution and non-ionic forms in alkaline solution by keeping a tautomerism equilibrium. Based on the presence of two kinds of molecular conformations in solution, the pH-sensitive phenomena of San and Che were explored. As depicted in Fig. 4, the fluorescence emission peaks at 582 nm and 570 nm decrease drastically until quenching with an increase of pH values, while the fluorescence emission peaks at 428 nm and 477 nm appear and increase gradually. The pH-dependent fluorescence emission behaviors indicate that the quaternary ammonium forms of San and Che have changed into non-ionic forms during the process. The experiment shows that San and Che display pH-sensitive behaviors in $CH_3OH/H_2O$ (v/v) mixtures which can be achieved by adjusting pH values.

Meanwhile, in view of the pH-dependent emission spectra, the p$K_a$ values of San and Che were calculated from the

Table 1 Photophysical data of San and Che in different $CH_3OH/H_2O$ (v/v) mixtures (20 μM)[a] at 25 °C

| Compound | Solvents | $\lambda_{abs}$/nm | $\lambda_{em}$/nm | $\Delta\lambda$/nm | Time/ns |
|---|---|---|---|---|---|
| San | $CH_3OH$ | 323 | 465 | 142 | 2.76 |
| | $CH_3OH/H_2O$ (5 : 5) | 321 | 578 | 257 | 3.05 |
| | $CH_3OH/H_2O$ (2 : 8) | 325 | 582 | 257 | 3.40 |
| Che | $CH_3OH$ | 320 | 461 | 141 | 2.95 |
| | $CH_3OH/H_2O$ (5 : 5) | 313 | 565 | 252 | 3.17 |
| | $CH_3OH/H_2O$ (1 : 9) | 312 | 570 | 258 | 3.27 |

[a] Stoke's shift calculated by $\Delta\lambda = \lambda_{em} - \lambda_{abs}$, $\lambda_{em}$: maximum emission wavelength at 25 °C, $\lambda_{abs}$: maximum absorption wavelength at 25 °C.

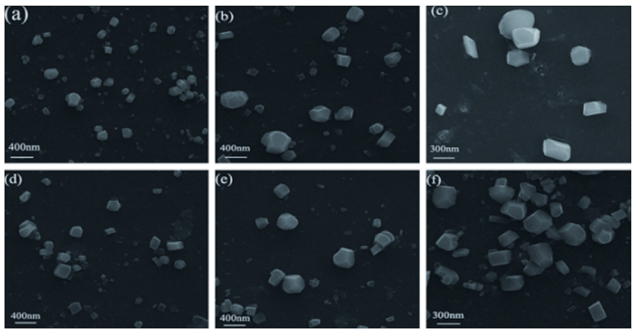


Fig. 3 TEM images of San and Che in $CH_3OH/H_2O$ (v/v) mixtures. (a) TEM image of San in $CH_3OH/H_2O$ (5 : 5) mixture. (b) TEM image of San in $CH_3OH/H_2O$ (3 : 7) mixture. (c) TEM image of San in $CH_3OH/H_2O$ (2 : 8) mixture. (d) TEM image of Che in $CH_3OH/H_2O$ (5 : 5) mixture. (e) TEM image of Che in $CH_3OH/H_2O$ (2 : 8) mixture. (f) TEM image of Che in $CH_3OH/H_2O$ (1 : 9) mixture.

sigmoidal fitting of the ratiometric emission. As shown in Fig. 4, the sigmoidal fitting yields a p$K_a$ value of 7.12 for San and 7.54 for Che. The p$K_a$ values are close to the intracellular pH values, which indicate that San and Che can be pH sensors for quantitative determination of intracellular pH. Moreover, the selectivity of San and Che to $H^+$ was examined to determine whether other cations are potential interferents. As shown in Fig. 5, it is noteworthy that San and Che show high selectivity toward $H^+$ over other cations. Besides, reversibility is another parameter to assess the performance of pH sensors. To examine whether the pH-dependent fluorescence emission behaviors of San and Che are reversible, pH values of solutions were adjusted back and forth between an acid environment and alkaline environment by using concentrated sodium hydroxide solution and hydrochloric acid, and the emission ratios of San and Che were recorded. As shown in Fig. 6, the results indicate that these processes are reversible and the response time is within seconds.

## Electronic distributions

The AIE(E) mechanism is explained by restricting nonradiative intramolecular rotation decay of excited molecules in the aggregation state. To understand the relationships between the

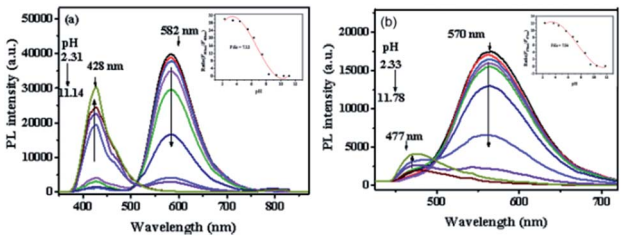


Fig. 4 Fluorescence emission spectra of San and Che at different pH values. (a) Change of fluorescence emission spectra of San ($c = 2.07 \times 10^{-5}$ M) with increasing pH from 2.31 to 11.14 in $CH_3OH/H_2O$ (2 : 8 v/v) mixture ($\lambda_{ex} = 385$ nm). Inset: sigmoidal fitting of the pH-dependent emission ($F_{582\ nm}/F_{428\ nm}$). (b) Change of fluorescence emission spectra of Che ($c = 2.07 \times 10^{-5}$ M) with increasing pH from 2.33 to 11.78 in $CH_3OH/H_2O$ (1 : 9 v/v) mixture ($\lambda_{ex} = 380$ nm). Inset: sigmoidal fitting of the pH-dependent emission ($F_{570\ nm}/F_{477\ nm}$).

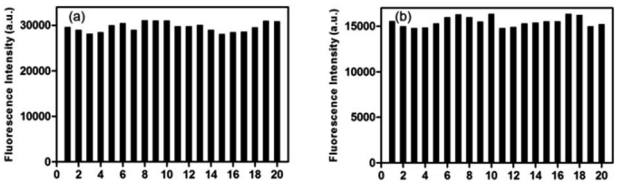


Fig. 5 The fluorescence intensity of San and Che (20 μM) in $CH_3OH/H_2O$ mixtures with diverse metal ions (200 μM), respectively. (a) The fluorescence intensity of San in $CH_3OH/H_2O$ (2 : 8 v/v) mixture at pH 6.3 with diverse metal ions. (b) The fluorescence intensity of Che in $CH_3OH/H_2O$ (1 : 9 v/v) mixture at pH 6.7 with diverse metal ions. (1) Blank; (2) $K^+$; (3) $Na^+$; (4) $Ag^+$; (5) $Ca^{2+}$; (6) $Mg^{2+}$; (7) $Ba^{2+}$; (8) $Fe^{2+}$; (9) $Cu^{2+}$; (10) $Zn^{2+}$; (11) $Mn^{2+}$; (12) $Ni^{2+}$; (13) $Co^{2+}$; (14) $Pb^{2+}$; (15) $Cd^{2+}$; (16) $Hg^{2+}$; (17) $Fe^{3+}$; (18) $Al^{3+}$; (19) $Cr^{3+}$; (20) $Li^+$. The fluorescence intensity is measured at $\lambda_{ex/em} = 385/582$ nm of San and $\lambda_{ex/em} = 380/570$ nm of Che.

AIEE behaviors and the electronic distributions of San and Che, the lowest unoccupied molecular orbital (LUMO) and the highest occupied molecular orbital (HOMO) of San and Che were calculated by density functional theory using Gaussian 09 program. As shown in Fig. 7, all optimized skeletons show conjugate plane structures. The HOMO energy level of San is calculated as −8.61 eV and the LUMO energy level is calculated as −5.79 eV; the energy gap is calculated to be 2.82 eV. Meanwhile, the HOMO energy level of Che is calculated as −9.08 eV and the LUMO energy level is calculated as −6.03 eV; the energy gap is calculated to be 3.05 eV. The energy gaps between the HOMO and LUMO of San and Che are in good agreement with the fluorescence emission wavelengths as shown in Fig. 1 and 2. Besides, the HOMO of San and Che are equably localized on entire molecular skeletons, while the LUMO are mainly localized on the isoquinoline part, which can facilitate adjacent molecules stacking in a "head to tail" pattern. The specific stacking mode is in accordance with the J-aggregation mechanism. Meanwhile, taking TEM images into consideration, the formation of J-aggregation is supposed to be responsible for the AIEE behaviors of San and Che.

## Application for mitochondrial imaging

Besides the remarkable AIEE nature of Che, cellular uptake behavior is also an important parameter for cell imaging. After

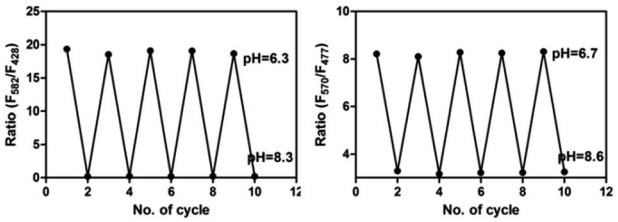


Fig. 6 Change in fluorescence intensity of San and Che between an acid environment and alkaline environment. (a) Change in fluorescence intensity of San between pH 6.3 and 8.3 ($\lambda_{ex} = 385$ nm). (b) Change in fluorescence intensity of Che between pH 6.7 and 8.6 ($\lambda_{ex} = 380$ nm).

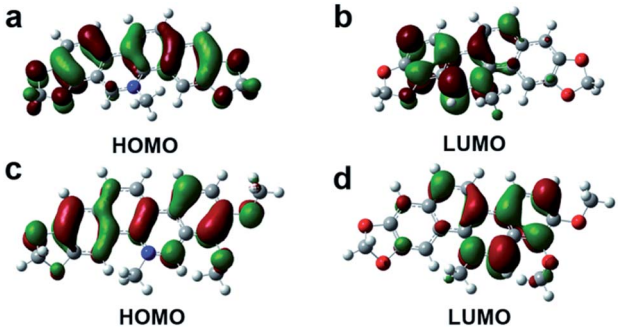


Fig. 7 Electronic distributions of San and Che. (a) HOMO distributions of San. (b) LUMO distributions of San. (c) HOMO distributions of Che. (d) LUMO distributions of Che.

incubation with Che (50 μM in serum free medium) for 30 minutes, strong blue and green fluorescence emission can be visualized in the cytoplasm region as illustrated in Fig. 8. It is established that when excited at 380 nm, Che displays two emission peaks which are located at 477 nm and 570 nm. The images coincide well with the fluorescence emission spectra of Che. Furthermore, strong fluorescence signals are exhibited after incubation for only 30 minutes. The fast cellular uptake indicates that Che can go through the cytomembrane and accumulate in some specific sub-cellular regions in a short time. To further ascertain the intracellular localization of Che, co-localization experiments with Mito Tracker Deep Red were performed by employing three different cell lines. As displayed in Fig. 9, green fluorescence signals from Che are overlapped well with red fluorescence signals from Mito Tracker by co-localization analysis, suggesting that Che is specifically located in the mitochondria of living cells. The Pearson correlation coefficient, indicative of the distribution correlation of two dyes ($R_r$: from −1 to 1), was introduced to quantify the staining region overlap between Che and Mito Tracker.[38] The coefficients are calculated as 0.95, 0.89, and 0.91, respectively, demonstrating the excellent mitochondrial targeting ability of Che.

## PH-sensitive cell imaging

As we can see in Fig. 4, the PL spectra of San and Che exhibit pH-sensitive behaviors. Because of the existence of both the non-ionic form and quaternary ammonium salt form in the

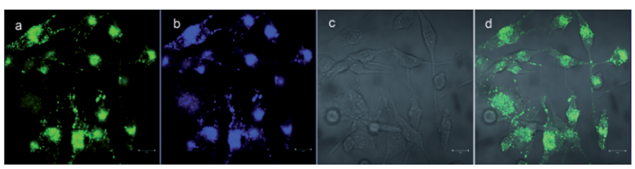


Fig. 8 CLSM images of $U_{87}$ cells incubated with 50 μM Che for 30 minutes. (a) Confocal image in green channel ($\lambda_{ex}$ = 405 nm, $\lambda_{em}$ = 500–560 nm). (b) Confocal image in blue channel ($\lambda_{ex}$ = 405 nm, $\lambda_{em}$ = 435–480 nm). (c) Bright-field image. (d) Merged image of (a)–(c). Scale bar = 20 μm.

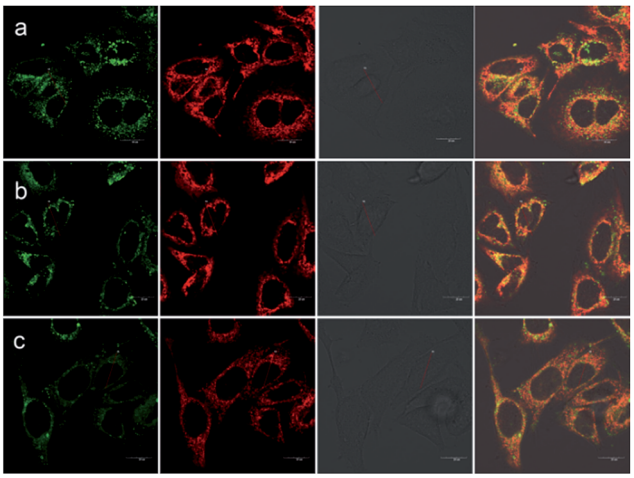


Fig. 9 Co-localized images of living cells stained with Che (50 μM) for 30 minutes and Mito Tracker Red (200 nM) for 15 minutes. (a) Co-localized images of RKO cells. (b) Co-localized images of $HepG_2$ cells. (c) Co-localized images of $U_{87}$ cells.

solution, a pH-sensitive cell imaging was performed to explore the effective form of Che for mitochondrial targeting. As illustrated in Fig. 10, the fluorescence emission intensity of Che in $U_{87}$ cells is in a pH-dependent manner. At pH = 6.0, strong green fluorescence is emitted. However, when pH values increase, the fluorescence emission intensity decreases gradually. This pH-dependent manner coincides well with the spectra as shown above and implies that an acidic environment favors cell imaging of Che. It has been established that both San and Che exist in two forms: a non-ionic form at high pH and a quaternary ammonium salt form at low pH. At pH = 6.0, most

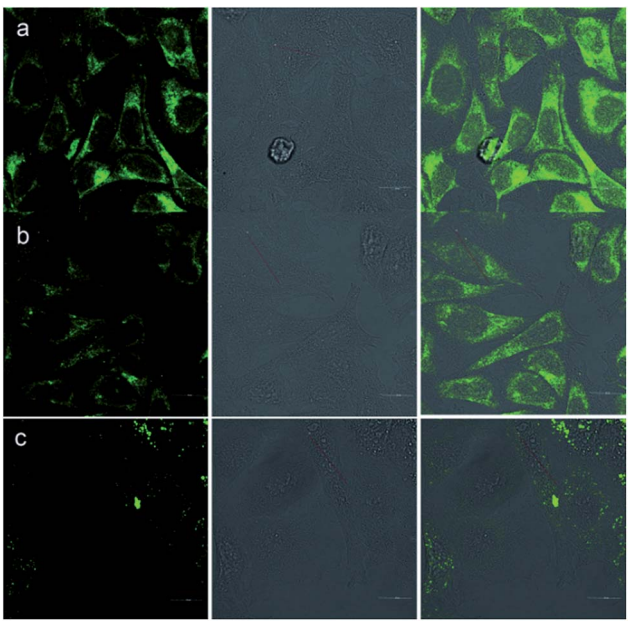


Fig. 10 CLSM images of $U_{87}$ cells incubated with Che (50 μM) for 30 minutes at different pH values. (a) pH = 6.0; (b) pH = 7.0; (c) pH = 8.0. Scale bar = 20 μm.

of Che exists in quaternary ammonium salt form. The quaternary ammonium salt form possesses a positive charge and can accumulate in mitochondria by an electrostatic driving force. However, at pH = 8.0, most of Che exist in the non-ionic form. The non-ionic form can't accumulate in mitochondria and so the fluorescence emission intensity decreases drastically. These results suggest the quaternary ammonium salt form is responsible for mitochondrial targeting and imaging. Studies have shown the extracellular microenvironment of tumor cells is weakly acidic and the mitochondrial membrane potential of tumor cells is more negative than normal cells,[39] which can facilitate Che diffusing into mitochondria as the quaternary ammonium salt form. Taking all these results into consideration, we can conclude the acidic extracellular microenvironment in tumor cells favors mitochondria-imaging of Che.

### Anti-cancer activities

It has been reported that San and Che can induce cell apoptosis in different cell lines, thus a cell viability assay was carried out. After incubation for 24 hours, the remarkable anti-cancer activities of San and Che are displayed. As is presented in Table 2, the growth of tumor cells is inhibited by San and Che with $IC_{50}$ values from 2 to 6 μM. The result confirms the anti-cancer activities of San and Che *in vitro*. Moreover, based on the superior mitochondria-targeting ability, the remarkable anti-cancer activities reported here imply San and Che-mediated cell death are related to mitochondrial dysfunction.

### Mitochondrial membrane potential changes and morphological changes

Studies have shown early mitochondria-mediated apoptosis mainly includes two aspects: depolarizing mitochondrial membrane potential and destroying morphologies of mitochondria, which are regarded as irreversible processes.[40] After confirming the unique AIEE property, high mitochondria-targeting performance and the remarkable anti-cancer activity of Che, we were interested in exploring its effect on mitochondrial membrane potential and morphology. As illustrated in Fig. 11a, 98.4% PBS-treated $U_{87}$ cells emit red fluorescence (FL2) compared with the negative control, indicating a higher mitochondrial membrane potential (MMP). However, in Che-treated $U_{87}$ cells, the green fluorescence emission (FL1) increases followed by a decrease of the red fluorescence emission (FL2), which suggests a decrease in mitochondrial membrane potential caused by Che. In conclusion, the flow cytometric analyses demonstrate that the aggregation of Che in mitochondria can depolarize mitochondrial membrane potential. To further explore morphological changes of mitochondria during the process, the AIEE nature of Che was employed to observe the dynamic changes. As shown in Fig. 11b, the reticulum-like and tubular-like mitochondria are transformed to dispersed small fragments with increasing scan time, indicative of collapses of mitochondrial structures.

What's more, the AIEE performance of Che disappears after 60 minutes. These results indicate that the aggregation of Che in mitochondria is destroyed by the decreasing MMP and the broken structures of mitochondria in $U_{87}$ cells. Taking together, Che can not only light up mitochondria but also induce mitochondrial dysfunction. In summary, as a unique AIEE molecule for mitochondrial imaging and targeting, Che was successfully explored for its anti-cancer activity through fluorescence imaging and is proposed to be a potential candidate of image-guided agents for anti-cancer studies.

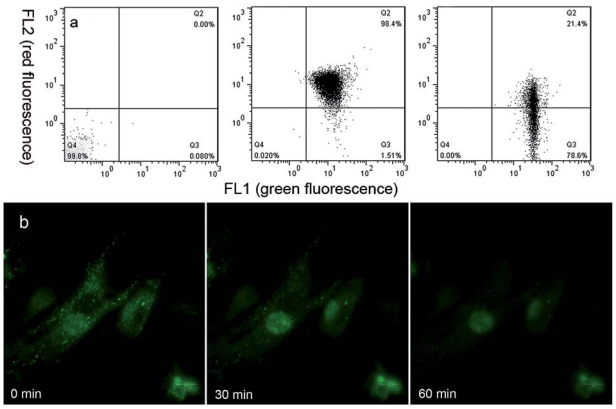


Fig. 11 Representative dot plots showing the fluorescence response for MMP and CLSM images of $U_{87}$ cells. (a) The dot plots of unstained $U_{87}$ cells, PBS-treated $U_{87}$ cells and Che-treated $U_{87}$ cells, respectively. (b) CLSM images of $U_{87}$ cells treated with Che (50 μM) with increasing scanning time.

Table 2 $IC_{50}$ values of tumor cells treatment with San and Che for 24 hours[a]

| Cell type | San (μM) | Che (μM) |
|---|---|---|
| $U_{87}$ | 2.4 | 3.3 |
| $HepG_2$ | 3.8 | 4.7 |
| RKO | 4.5 | 5.6 |

[a] Data are shown as the mean values of three independent experiments.

## Experimental section

### Materials and apparatus

Sanguinarine chloride hydrate (>98% purity), chelerythrine chloride (>98% purity) were purchased from Sigma-Aldrich (St. Louis, MO, USA) and used as received. All other chemicals were analytical grade and used without further purification. The human glioma cell line $U_{87}$, colon cancer cell line RKO, and hepatocellular carcinoma cell line $HepG_2$ were purchased from laboratory animal center of Sun Yat-sen University. Dulbecco's modified Eagle's medium (DMEM), Roswell Park Memorial Institute 1640 medium (RPMI-1640), fetal bovine serum (FBS), phosphate buffered saline (PBS), 0.25% trypsin solution, penicillin-streptomycin solution, Mitotracker Red assay kit (MT), and 5,5′,6,6′-tetrachloro-1,1′,3,3′-tetraethylimidacarbocyanine iodide (JC-1) assay kit were purchased from Thermo-Fisher Biochemical Products (Beijing, China) Co., Ltd. Nigericin was purchased from Invitrogen (Carlsbad, CA). Ultrapure water was obtained from a Milli-Q Plus System

(Millipore Corporation, USA). All pH were measured using a PHS-3C pH meter. Photoluminescence (PL) spectra were recorded on a FLS 920 spectrophotometer (Edinburgh Instruments, England). Fluorescence lifetime was collected on a FLS 980 spectrometer (Edinburgh Instruments, England). Ultraviolet absorption spectra were tested on a Shimadzu UV-2600 spectrometer (Shimadzu, Japan). Transmission electron microscope (TEM) images were collected on a Zeiss Merlin transmission electron microscope (Zeiss, Germany). Flow cytometric analyses were conducted by a Cell Lab Quanta SC-MPL flow cytometer (Beckman Coulter, USA). Fluorescent images were taken on a LSM 710 laser scanning confocal microscope (Zeiss, Germany) and analyzed by ZEN 2009 software.

### Preparations for UV-vis spectra, PL spectra and TEM measurements

1.53 mg San and 1.59 mg Che were separately dissolved in methanol to make stock solutions at a concentration of $2.07 \times 10^{-4}$ M; then, aliquot stock solutions of San and Che were mixed with appropriate amounts of methanol and water. A series of solutions at a concentration of $2.07 \times 10^{-5}$ M were finally prepared with water fractions increasing from 0 to 90 vol%. UV-vis absorption spectra and PL spectra of San and Che were measured at room temperature. Excitation and emission bandwidths were both set at 3 nm; the excitation wavelength was 385 nm for San and 380 nm for Che. The PL spectra at different pH values were also tested by adjusting pH values from 1 to 11 in $CH_3OH/H_2O$ (2 : 8, v/v) mixture of San and $CH_3OH/H_2O$ (1 : 9, v/v) mixture of Che. The fluorescence lifetime of San in $CH_3OH$, $CH_3OH/H_2O$ (5 : 5, v/v) mixture, $CH_3OH/H_2O$ (2 : 8, v/v) mixture, and Che in $CH_3OH$, $CH_3OH/H_2O$ (5 : 5, v/v) mixture, $CH_3OH/H_2O$ (1 : 9, v/v) mixture were measured by a FLS 980 spectrometer. As far as the morphologies of the aggregation were concerned, drops of $CH_3OH/H_2O$ (5 : 5, 3 : 7, and 2 : 8 v/v) solutions of San and $CH_3OH/H_2O$ (5 : 5, 2 : 8, and 1 : 9 v/v) solutions of Che were put on a silicon wafer over 12 h at room temperature for slow evaporation, then metal spraying was performed for TEM imaging after completely drying.

### Theoretical calculations

To better understand the relationships between the optical properties and electronic structures of San and Che, the natural bond orbital charge distributions of the highest occupied molecular orbital (HOMO) and the lowest unoccupied molecular orbital (LUMO) were calculated by density functional theory (DFT) using Gaussian 09 program at B3LYP/6-31G* level.

### Cellular uptake and co-localization experiments

$U_{87}$ cells, $HepG_2$ cells, and RKO cells were cultured in DMEM culture medium or RPMI-1640 culture medium containing 10% heat-inactivated fetal bovine serum, 100 units $mL^{-1}$ penicillin, and 100 μg $mL^{-1}$ streptomycin in an incubator with 5% $CO_2$ at 37 °C. Cells were used at 80% confluence before experiments. To evaluate cell membrane permeability, Che was chosen to explore the cellular uptake behavior because of its better AIEE performance. In brief, $1 \times 10^5$ $U_{87}$ cells were incubated with Che (50 μM in serum-free medium) for 30 minutes. After rinsing with fresh PBS (pH = 7.4) three times, the fluorescence was examined with a confocal laser scanning microscope using a 100 oil-immersion objective lens and the results were imaged using various combinations of excitation wavelength and emission wavelengths. Compared with the commonly reported mitochondria-targeting groups, such as triphenylphosphonium, pyridine, and quinoline, Che was supposed to accumulate in mitochondria as a lipophilic cation. Therefore, co-localization experiments were performed to assess its capability for mitochondria-targeting. First, cells were treated with 50 μM Che for 30 minutes and co-stained with 200 nM Mito Tracker Deep Red (a commercially available mitochondrial dye) for 15 minutes, then excess dyes were rinsed away by PBS solution for 2–3 times. Finally, the fluorescence was detected by a confocal laser scanning microscope and results were imaged using various combinations of excitation wavelengths and emission wavelengths. All procedures were performed away from light.

### The effect of pH on cell imaging and cell viability assay

Based on the fact that both San and Che undergo pH-sensitive properties in $CH_3OH/H_2O$ mixtures, the effect of different pH values on cell imaging was explored in this study. $U_{87}$ cells were first incubated with 50 μM Che in DMEM culture medium for 30 minutes. After removing the staining solutions, different PBS buffers (pH = 6.0, 7.0, and 8.0) were added into three dishes, respectively. Then nigericin solutions were added and cells were incubated for 15 minutes to equilibrate intracellular and extracellular pH values. Three different pH gradients (pH = 6.0, 7.0, and 8.0) were established to mimic cellular pH conditions and images were acquired on a confocal fluorescence microscope. The excitation wavelength was 405 nm and the emission wavelength was 500–560 nm. We were interested to evaluate the anti-cancer activities of San and Che; thus, a CCK-8 cell viability assay was performed. Tumor cells were seeded in 96-well plates at a density of $5 \times 10^3$ cells per well and 24 hours later, Che and San at concentrations of 1, 2, 4, 8, and 16 μM were added to the wells. After 24 hours, each well was treated with 10 μL of prepared CCK-8 solution and the cells were incubated for an additional 2 hours at 37 °C. The absorbance value of each well was recorded on a PerkinElmer Victor plate reader at 450 nm and the following equation was employed to calculate the cell viability: percentage of viable cells: (%) = (mean absorbance value of the treatment group/mean absorbance value of the negative control group) × 100%. Cells incubated with the culture medium instead of Che and San solutions were defined as the negative control group. The experiment was tested at least three times.

### Mitochondrial membrane potential changes and morphological changes

To evaluate whether the aggregation of Che in mitochondria was involved in mitochondrial dysfunction, mitochondrial membrane potential (MMP) was detected by 5,5′,6,6′-tetrachloro-1,1′,3,3′-tetraethyl-imidacarbocyanine iodide (JC-1). JC-1

is a specific mitochondrial dye with green-red fluorescence. When mitochondrial membrane potential is at a high level, JC-1 can accumulate in a mitochondrial matrix and emit red fluorescence. However, when the integrity of a mitochondrial membrane is damaged, then JC-1 can't accumulate in a mitochondrial matrix and emit green fluorescence at that moment. Therefore, color conversion between green and red can be an indicator of the mitochondrial membrane potential change. To assess the effect of Che on MMP, living $U_{87}$ cells were incubated with 50 μM Che for 30 minutes followed by the reaction with 200 μL of JC-1 solutions (10 μg $mL^{-1}$) for another 15 minutes, then excess JC-1 solutions were rinsed away by PBS solutions for 2–3 times and the MMP of $U_{87}$ cells was assessed by flow cytometry. During each flow cytometric analysis, $1 \times 10^4$ $U_{87}$ cells were analyzed at the slowest flow rate. Data were displayed as two-dimensional dot plots and the background particles were excluded by the use of gates and thresholds. In particular, living $U_{87}$ cells treated with PBS solutions instead of Che were set to negative controls. After investigating the MMP change caused by Che, morphological changes of mitochondria were also monitored by utilizing the AIEE characteristic of Che. As mentioned above, living $U_{87}$ cells were stained with 50 μM Che for 30 minutes to realize cellular uptake, then fluorescent images were collected by a confocal fluorescence microscope with increasing scan time.

## Conclusions

In this paper, chelerythrine and sanguinarine were explored for their aggregation-induced emission enhancement (AIEE) characteristics. After adding increasing amounts of $H_2O$ to $CH_3OH$ solutions of San and Che, typical AIEE behaviors could be observed. Furthermore, the fluorescence lifetime in $CH_3OH/H_2O$ mixtures confirmed the AIEE characteristics. Moreover, the physical forms with different water ratios were also examined, demonstrating the formation of light-emitting nanoparticles. By DFT calculations, J-aggregation proved to be responsible for the AIEE behaviors of San and Che. Because of the existence of non-ionic forms and quaternary ammonium salt forms in solution, San and Che displayed pH-sensitive behaviors. Besides, satisfactory photostability, reversibility, and selectivity of San and Che were displayed, indicating they have considerable potentials as pH sensors. Taking advantage of the AIEE characteristics and pH-sensitive properties, high specificity to mitochondria of Che was displayed as the quaternary ammonium salt form. Moreover, after confirming the anti-cancer effects of San and Che, the depolarization of mitochondrial membrane potential and morphological collapses of mitochondrial structures were observed, proving mitochondrial dysfunction caused by Che. Therefore, these results not only explained the anti-cancer effect of Che through fluorescence imaging but also presented a potential image-guided therapeutic reagent. In future work, we will focus on the development of simple and efficient natural products for mitochondrial imaging and manipulating with AIEE characteristics.

## Conflicts of interest

There are no conflicts to declare.

## Acknowledgements

This work was supported by the National Natural Science Foundation of China (Grant number: 81774099 and 81173577), the National Key R&D Program of China (2017YFC1701100) and the Natural Science Foundation of Guangdong (8451008901000380).

## Notes and references

1 J. Nunnari and A. Suomalainen, *Cell*, 2012, **148**, 1145–1159.
2 J. Palmfeldt and P. Bross, *Mitochondrion*, 2017, **33**, 2–14.
3 J. R. Friedman and J. Nunnari, *Nature*, 2014, **505**, 335–343.
4 N. S. Chandel, *Cell Metab.*, 2015, **22**, 204–206.
5 S. Vyas, E. Zaganjor and M. C. Haigis, *Cell*, 2016, **166**, 555–566.
6 T. Bek, *Mitochondrion*, 2017, **36**, 4–6.
7 A. Grimm, A. G. Mensah-Nyagan and A. Eckert, *Neurosci. Biobehav. Rev.*, 2016, **67**, 89–101.
8 D. Senft and A. R. Ze'ev, *Curr. Opin. Cell Biol.*, 2016, **39**, 43–52.
9 M. Bayeva, M. Gheorghiade and H. Ardehali, *J. Am. Coll. Cardiol.*, 2013, **61**, 599–610.
10 A. Logan, V. R. Pell, K. J. Shaffer, C. Evans, N. J. Stanley, E. L. Robb and S. Vidoni, *Cell Metab.*, 2016, **23**, 379–385.
11 I. Martínez-Reyes, L. P. Diebold, H. Kong, M. Schieber, H. Huang, C. T. Hensley and E. Dufour, *Mol. Cell*, 2016, **61**, 199–209.
12 B. Kalyanaraman, G. Cheng, M. Hardy, O. Ouari, M. Lopez, J. Joseph and M. B. Dwinell, *Redox Biol.*, 2017, **14**, 316–327.
13 J. Zielonka, J. Joseph, A. Sikora, M. Hardy, O. Ouari, J. Vasquez-Vivar and B. Kalyanaraman, *Chem. Rev.*, 2017, **117**, 10043–10120.
14 H. Zhu, J. Fan, J. Du and X. Peng, *Acc. Chem. Res.*, 2016, **49**, 2115–2126.
15 J. Luo, Z. Xie, J. W. Y. Lam, L. Cheng, H. Chen, C. Qiu and B. Z. Tang, *Chem. Commun.*, 2001, 1740–1741.
16 S. Yang, W. Shen, W. Li, J. Tang, W. Yao, J. Wang and Z. Xu, *RSC Adv.*, 2016, **6**, 74225–74233.
17 L. Zhou, D. Xu, H. Gao, A. Han, Y. Yang, C. Zhang and F. Zhao, *RSC Adv.*, 2016, **6**, 69560–69568.
18 D. Ding, K. Li, B. Liu and B. Z. Tang, *Acc. Chem. Res.*, 2013, **46**, 2441–2453.
19 C. W. T. Leung, Y. Hong, S. Chen, E. Zhao, J. W. Y. Lam and B. Z. Tang, *J. Am. Chem. Soc.*, 2013, **135**, 62–65.
20 T. K. Ryan, Y. Y. Chris, W. Y. Jacky and B. Z. Tang, *Chem. Commun.*, 2015, **51**, 9022–9025.
21 N. Zhao, S. Chen, Y. Hong and B. Z. Tang, *Chem. Commun.*, 2015, **51**, 13599–13602.
22 C. W. T. Leung, Y. Hong and B. Z. Tang, *Methods Mol. Biol.*, 2015, **1208**, 21–27.
23 X. Gu, E. Zhao, J. W. Y. Lam, Q. Peng, Y. Xie, Y. Zhang and B. Z. Tang, *Adv. Mater.*, 2015, **27**, 7093–7100.
24 F. Hu and B. Liu, *Org. Biomol. Chem.*, 2016, **14**, 9931–9944.

 

25 Q. Hu, M. Gao, G. Feng and B. Liu, *Angew. Chem., Int. Ed.*, 2014, **53**, 14225–14229.
26 C. J. Zhang, Q. Hu, G. Feng, R. Zhang, Y. Yuan, X. Lu and B. Liu, *Chem. Sci.*, 2015, **6**, 4580–4586.
27 Q. Hu, M. Gao, G. Feng, X. Chen and B. Liu, *ACS Appl. Mater. Interfaces*, 2015, **7**, 4875–4882.
28 G. Yu, D. Wu, Y. Li, Z. Zhang, L. Shao, J. Zhou and F. Huang, *Chem. Sci.*, 2016, **7**, 3017–3024.
29 Z. X. Qing, P. Yang, Q. Tang, P. Cheng, X. B. Liu, Y. J. Zheng and J. G. Zeng, *Curr. Org. Chem.*, 2017, **21**, 1920–1934.
30 A. Burgeiro, A. C. Bento, C. Gajate, P. J. Oliveira and F. Mollinedo, *Eur. J. Pharmacol.*, 2013, **705**, 109–118.
31 S. Kumar and A. Acharya, *Tumor Biol.*, 2014, **35**, 129–140.
32 X. Tang, J. Zhang, L. Liu, D. Yang, H. Wang and F. He, *J. Photochem. Photobiol., A*, 2017, **337**, 71–81.
33 L. Huang, A. Shi, F. He and X. Li, *Bioorg. Med. Chem.*, 2010, **18**, 1244–1251.
34 A. Shi, L. Huang, C. Lu, F. He and X. Li, *Bioorg. Med. Chem.*, 2011, **19**, 2298–2305.
35 L. Huang, T. Su, W. Shan, Z. Luo, Y. Sun, F. He and X. Li, *Bioorg. Med. Chem.*, 2012, **20**, 3038–3048.
36 M. Liu, K. Wang, X. Zhang, X. Zhang, Z. Li, Q. Zhang and Y. Wei, *Tetrahedron*, 2015, **71**, 5452–5457.
37 A. B. Pradhan, S. Bhuiya, L. Haque, R. Tiwari and S. Das, *Spectrochim. Acta, Part A*, 2017, **170**, 89–96.
38 M. Y. Wu, K. Li, Y. H. Liu, K. K. Yu, Y. M. Xie, X. D. Zhou and X. Q. Yu, *Biomaterials*, 2015, **53**, 669–678.
39 D. C. Wallace, *Nat. Rev. Cancer*, 2012, **12**, 685–698.
40 S. Xiong, T. Mu, G. Wang and X. Jiang, *Protein Cell*, 2014, **5**, 737–749.